THE JOURNAL OF PHYSICAL CHEMISTRY Letters

Letter

pubs.acs.org/JPCL

Variance Spectroscopy

Jason K. Streit,[†,§] Sergei M. Bachilo,[†] Stephen R. Sanchez,[†] Ching-Wei Lin,[†] and R. Bruce Weisman*[,†,‡]

[†]Department of Chemistry and the Smalley-Curl Institute and [‡]Department of Materials Science and NanoEngineering, Rice University, 6100 Main Street, Houston, Texas 77005, United States

Supporting Information

ABSTRACT: Spectroscopic analysis and study of nanoparticle samples is often hampered by structural diversity that presents a complex superposition of spectral signatures. By probing the spectra of small volumes within dilute samples, we can expose statistical variations in composition to obtain information unavailable from bulk spectroscopy. This new approach is demonstrated using fluorescence spectra of unsorted single-walled carbon nanotube samples to deduce structure-specific abundances and emissive efficiencies. Furthermore, correlations between intensity variations at different wavelengths provide two-dimensional covariance maps that isolate the spectra of homogeneous subpopulations. Covariance analysis is also a sensitive probe of particle aggregation. It shows that well-dispersed nanotube samples can spontaneously form loose aggregates of a type not previously recognized. Variance spectroscopy is a simple and practical technique that should find application in many nanoparticle studies.

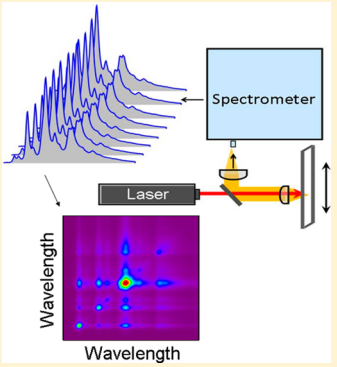

Methods of bulk spectroscopy normally probe such large numbers of particles that they cannot detect spatial or temporal signal variations reflecting the granularity of matter. However, fluorescence correlation spectroscopy and a family of related techniques deliberately interrogate small volumes of dilute samples in order to capture fluctuations in the number of particles and deduce information about particle concentration and diffusional mobility.[1−4] To date, these fluctuation methods have typically examined intensity changes in spectrally unresolved fluorescence, extracting little or no information in the wavelength regime. However, careful spectral analysis of intensity fluctuations is potentially quite useful for studying nanomaterials, which often contain a variety of particle sizes or structures and show corresponding heterogeneity in their spectra. As an important and obvious example, samples of unsorted single-walled carbon nanotubes (SWCNTs) display numerous distinct and structure-specific fluorescence emission features corresponding to the various structural species that are present.[5−7] We describe here a method, termed variance spectroscopy, for measuring and analyzing wavelength-dependent intensity fluctuations in the emission from such samples to reveal abundances, emission efficiencies, homogeneous subpopulation spectra, and aggregation processes.

Inhomogeneous fluid samples will show spectral variations in time as the composition of a small observed volume changes through particle diffusion. Alternatively, spectral variations can be observed in the spatial regime by comparing spectra of different small regions of a bulk sample using "snapshots" fast enough to prevent diffusional averaging of the composition. In this study we demonstrate variance spectroscopy in the spatial regime using fluorescence. We acquire measurements on very small regions of diluted bulk samples to limit the numbers of sample particles of each type inside the observation volume. Efficient optical collection and sensitive detection allow emission signals to dominate instrumental noise at the required short integration times. To measure spectra from different spatial regions, we either flow liquid samples smoothly through a fixed optical cell, or use a static sample in a closed cell that is mechanically translated across the interrogation beam.

Unsorted samples of individually dispersed SWCNTs are known to show complex fluorescence spectra in the short-wave infrared (SWIR) region following excitation at visible wavelengths.[5] These spectra are superpositions of features from multiple structural species of semiconducting SWCNTs, each of which is designated by a pair of integers, (n,m), and emits at a known characteristic peak wavelength.[6,8] To measure a variance spectrum, we prepare a well-dispersed liquid suspension of SWCNTs at a concentration near 0.5 μg/mL (~0.5 ppm by mass). The beam from a visible diode laser is tightly focused into a thin sample cell to excite a volume of approximately 5 pL. Emission from this sample region is captured by a lens with numerical aperture near 0.5 and transmitted to a SWIR spectrometer containing a 512-channel InGaAs detector array. We acquire a sequence of approximately 2000 spectra with integration times of 200 ms or less at intervals that ensure that each spectrum represents a distinct region in the sample. A set of spectra is typically collected within 30 min.

The data set is analyzed using moment analysis[9,10] to compute the mean fluorescence intensity, $\overline{I}(\lambda)$, and the squared standard deviation, or variance, $\sigma^2(\lambda)$, separately for each wavelength channel. Under our experimental conditions, the variance is dominated by statistical sample variations rather

Received: August 21, 2015
Accepted: September 18, 2015
Published: September 18, 2015

DOI: 10.1021/acs.jpclett.5b01835
J. Phys. Chem. Lett. 2015, 6, 3976−3981

than instrumental noise (see Supporting Information). Nevertheless, to remove the small contribution from detector readout noise we correct all points in the variance spectrum by subtracting the average variance values in dark detector channels. In the absence of instrumental contributions, the ratio of standard deviation to mean intensity is determined by $N(\lambda)$, the mean number of observed particles contributing to emission at λ, according to eq 1:

$$\frac{\sigma(\lambda)}{\overline{I}(\lambda)} = \frac{\sqrt{N(\lambda)}}{N(\lambda)} = \frac{1}{\sqrt{N(\lambda)}} \tag{1}$$

The variance spectrum can therefore be expressed as

$$\sigma^2(\lambda) = \frac{\overline{I}^2(\lambda)}{N(\lambda)} \tag{2}$$

Figure 1 shows an example of mean and variance spectra measured for an unsorted sample of HiPco SWCNTs dispersed

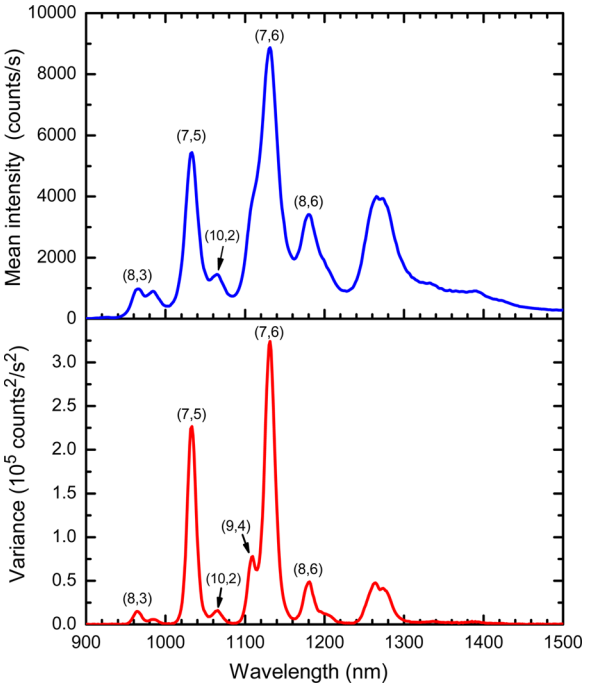

Figure 1. Mean and variance spectra from an unsorted SWCNT sample. The aqueous sodium deoxycholate dispersion of HiPco SWCNTs was flowed slowly through a fixed cell and excited at 642 nm. (Top) Mean of 3000 spectra. (Bottom) Variance spectrum computed from the same data set. Features assigned to specific (n,m) species are labeled.

in aqueous sodium deoxycholate surfactant. A common and challenging task when working with such samples is finding the relative abundances of the various emissive (n,m) species that are present. To extract those abundances from our data, we note that for well-dispersed samples with individualized nanotubes, both the mean and variance spectra are superpositions of contributions from the different species:

$$\overline{I}(\lambda) = \sum_{(n,m)} \overline{I}_{(n,m)}(\lambda) = \sum_{(n,m)} \mathbf{n}_{(n,m)} i_{(n,m)}(\lambda) \tag{3}$$

$$\sigma^2(\lambda) = \sum_{(n,m)} \sigma^2_{(n,m)}(\lambda) = \sum_{(n,m)} \frac{[\overline{I}_{(n,m)}(\lambda)]^2}{\mathbf{n}_{(n,m)}} = \sum_{(n,m)} \mathbf{n}_{(n,m)} [i_{(n,m)}(\lambda)]^2 \tag{4}$$

Here, $i_{(n,m)}(\lambda)$ represents the emission spectrum of one nanotube of species (n,m) and $\mathbf{n}_{(n,m)}$ is the number of such nanotubes in the observed volume. We apply eqs 3 and 4 to fit the experimental mean and variance spectra using $i_{(n,m)}(\lambda)$ functions with peak positions, widths, and shapes consistent with those found from prior SWCNT spectral studies.[11] The individual components and overall fits deduced for a pair of mean and variance spectra are shown along with data points in Figure 2. This simulation process provides amplitudes for the

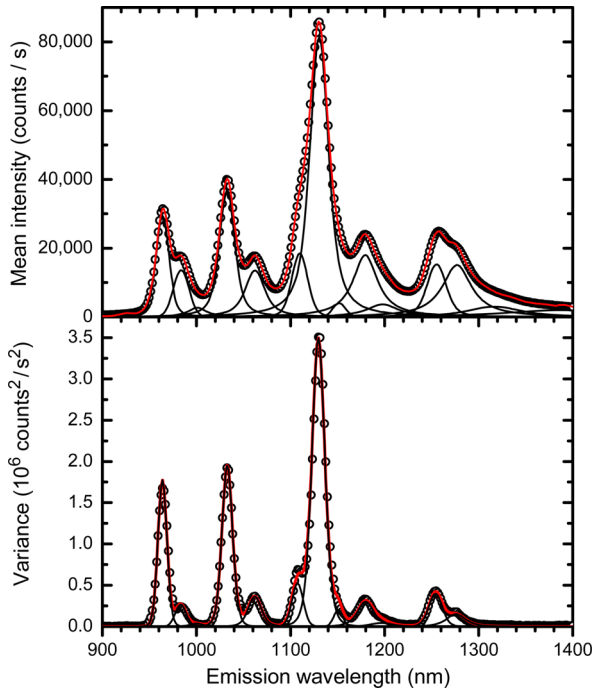

Figure 2. Spectral simulations of mean and variance spectra from an unsorted SWCNT sample. A static cell holding an aqueous sodium deoxycholate dispersion of HiPco SWCNTs was translated relative to the optical system and excited at 660 nm. A total of 2150 spectra were acquired to obtain the mean (top) and variance (bottom) spectra. Each frame shows measured data (circles), overall simulation (solid red curve), and individual (n,m) components (solid black curves).

set of $i_{(n,m)}(\lambda)$, giving the relative emission efficiencies for the different nanotube species when excited at the laser wavelength used in the experiment (see Supporting Information). The spectral fitting also reveals the sample's composition by determining its set of structure-specific particle abundances, $\mathbf{n}_{(n,m)}$, which are very challenging to find by other methods. To confirm that these abundance values are not distorted by instrumental contributions to variance spectra, we analyzed a SWCNT dispersion before and after it was diluted by volumetric factors of 1.4 and 2.0. The deduced abundance changes for six different (n,m) species all match the known volumetric factors to within 4% (see Supporting Information).

Variance data can be further analyzed to generate two-dimensional spectra representing correlations between intensity fluctuations at different wavelengths. This is conceptually

DOI: 10.1021/acs.jpclett.5b01835
J. Phys. Chem. Lett. 2015, 6, 3976−3981

related to fluorescence cross-correlation spectroscopy,[12−15] which compares time fluctuations in different spectral regions to study the formation of complexes, and also to 2D correlation spectroscopy,[16,17] in which the strengths of spectral features (typically vibrational) are analyzed for time correlations in externally perturbed samples. In our spatiospectral measurements on fully dispersed samples, any two spectral channels will show a positive correlation only if emission at both wavelengths comes from the same subpopulation, such as a single (n,m) species of nanotube. By contrast, two spectral channels arising from different species will show zero correlation because the random concentration variations of those species will be independent. However, samples with some degree of aggregation may contain clusters that include species of different types and show composite emission spectra. Variations in the concentrations of such clusters will then give positively correlated changes in the intensities of those component spectral channels. Negative correlations might appear when the population of a species is partitioned between two environments that give distinguishable spectra.

To quantify correlated intensity changes, we calculate the covariance matrix for all pairs of wavelengths, (λ_j, λ_k), over the data set of M spectra:

$$\mathrm{cov}(\lambda_j, \lambda_k) = \frac{\sum_{i=1}^{M} (I_i(\lambda_j) - \bar{I}(\lambda_j))(I_i(\lambda_k) - \bar{I}(\lambda_k))}{M} \quad (5)$$

As illustrated in Figure 3a, the results can be visualized as a two-dimensional contour plot in which each axis is emission wavelength. Values along the diagonal trace the variance spectrum described earlier, and reflection symmetry across that diagonal line is imposed by the definition of covariance. A horizontal or vertical profile taken at some wavelength in the covariance plot reveals the set of spectral features that are correlated with the chosen wavelength. If no aggregates are present, it can be shown (see Supporting Information) that the profile is a linear superposition of mean fluorescence spectra from all (n,m) species in the sample, with each weighted by the ratio of its fluorescence intensity at the chosen wavelength to the number of (n,m) particles (its emissive efficiency at that wavelength under the experimental excitation conditions). If the wavelength is near the emission peak of one species, then the profile can be strongly dominated by the spectrum of that single species. Also, particles in the sample that emit weakly (including damaged nanotubes or impurities) will contribute very little to the covariance spectral profile, even if they are present at high abundances and collectively give a significant amount of emission. To illustrate covariance profile analysis, the red curve in Figure 3b shows a profile at the peak emission wavelength of (7,6) SWCNTs for a well-dispersed sample. It properly reveals a weak emission sideband near 1290 nm that is totally obscured by spectral congestion in the mean and variance emission spectra. For reference, the nearly identical black curve in Figure 3b shows the emission spectrum from an individual (7,6) SWCNT, as measured under a SWIR fluorescence microscope.[18] The strong similarity of these spectra demonstrates the effectiveness of covariance analysis for faithfully extracting the spectrum of one subpopulation of particles within a highly heterogeneous sample. By measuring variance spectra with two additional excitation wavelengths and then selecting covariance profiles at the emission peaks of different (n,m) species, we obtained the set of normalized emission profiles shown in Figure 3c. Although this

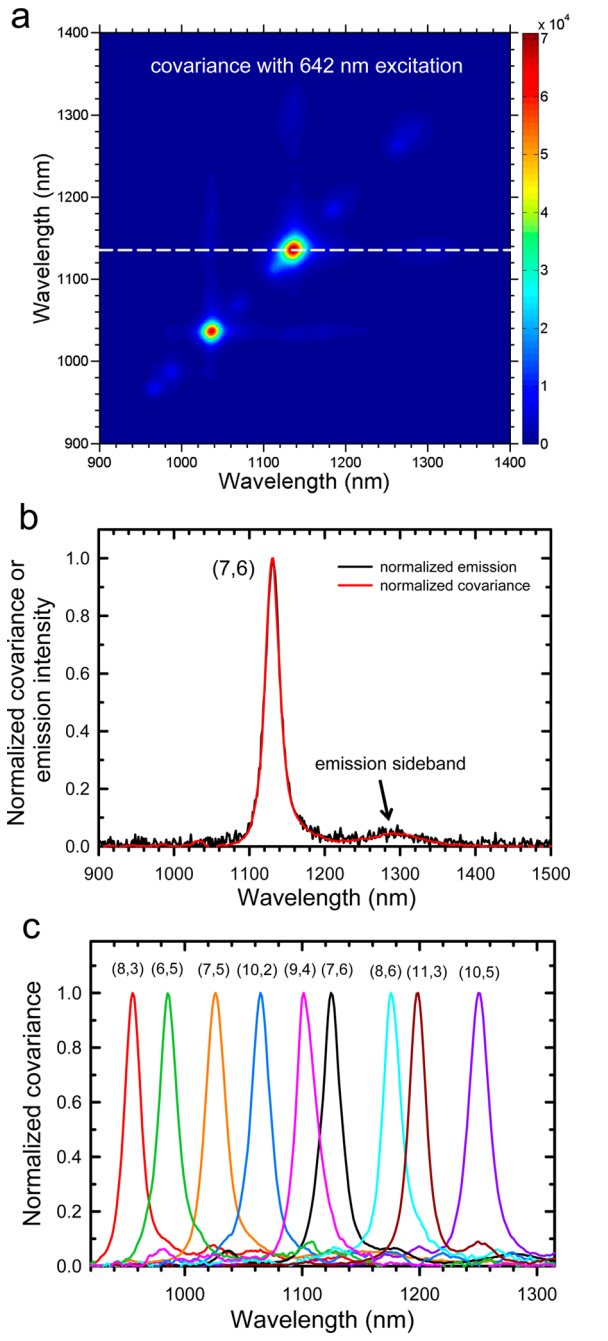

Figure 3. Covariance analyses. (a) Covariance matrix computed from the data set of Figure 1, plotted as a contour map. The dashed white line marks the profile plotted in frame b. (b) Covariance spectrum at the peak wavelength of (7,6) emission (red curve) and fluorescence spectrum of an individual (7,6) SWCNT measured separately under a microscope (black curve). (c) Normalized covariance spectra at the peak wavelengths of the nine labeled (n,m) species, compiled from covariance matrices measured from an unsorted SWCNT sample using excitation at 642, 659, and 784 nm.

fluorescence-based method will not detect the minority of SWCNT species that are metallic (nonemissive), to our knowledge it is the only simple spectroscopic technique that can measure single-species spectra with such clarity from mixed bulk samples.

In the absence of energy transfer or fluorescence quenching processes, aggregation of some or all of the particles in a sample should lead to covariance plots with intensified diagonal peaks

DOI: 10.1021/acs.jpclett.5b01835
J. Phys. Chem. Lett. 2015, 6, 3976−3981

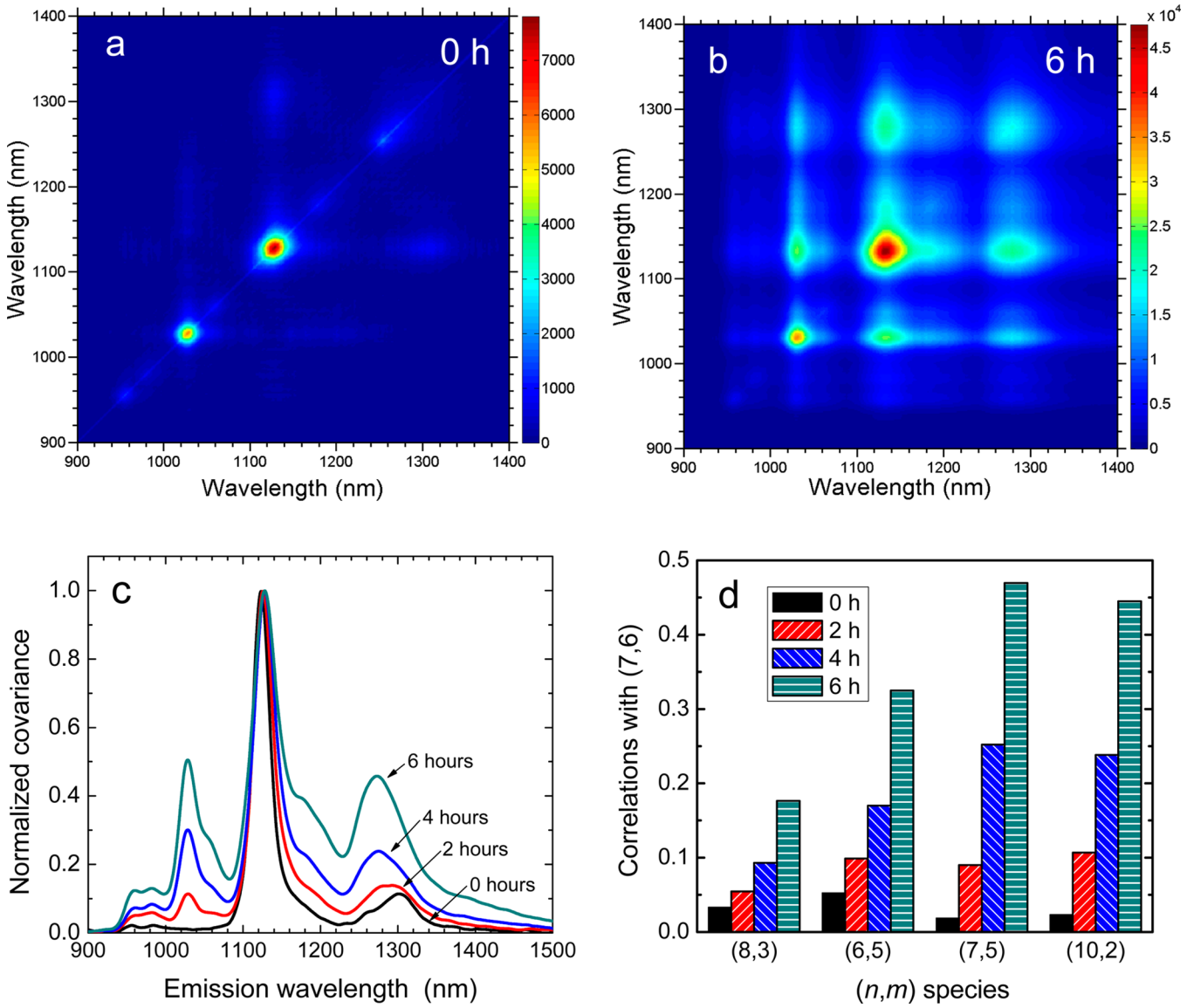

Figure 4. Aggregation monitored by covariance analysis. (a) Covariance matrix of an aqueous dispersion of SWCNTs in sodium dodecyl sulfate. The sample was excited at 642 nm. (b) Covariance matrix of the same sample measured 6 h after the addition of NaCl. Note change of intensity scale. (c) Normalized covariance spectra at the (7,6) peak emission wavelength at the labeled delays after NaCl addition. (d) Scaled correlation coefficients showing estimated fractions of (7,6) SWCNTs aggregated with four other (n,m) species at different times after NaCl addition.

and new off-diagonal features. To confirm this, we began with a sample of SWCNTs well-dispersed in a solution of sodium dodecyl sulfate surfactant. NaCl was then added to induce aggregation of this ionic colloid,[19] and the sample was monitored by variance spectroscopy at 2 h intervals. Figure 4a,b shows the covariance plots at 0 and 6 h. Diagonal peaks are intensified several-fold, indicating higher variances resulting from decreased numbers of emitting particles. This implies that many nanotubes of a specific (n,m) species have become physically linked to others of the same type. In addition, the matrix measured at 6 h displays strong off-diagonal features arising from aggregates that contain nanotubes of different (n,m) species with normal emissive properties. We refer to these previously unrecognized particles as "loose" aggregates to distinguish them from the familiar tight bundles in which nanotubes closely bound to each other by van der Waals forces show strong spectral perturbations from altered dielectric environment, energy transfer between semiconducting nanotubes, and quenching by metallic nanotubes.[5,20−23] Growth of the off-diagonal spectral features reflecting loose aggregates can be seen from normalized covariance spectra measured at the (7,6) emission peak (Figure 4c), which show systematic increases near the emission peaks of other (n,m) species. There are also more subtle changes in the main peak near 1125 nm (see Figure S8). To quantify the growth of off-diagonal features, we computed scaled Pearson correlation coefficients describing the fraction of particles with emission wavelength λ_j that are aggregated with the species emitting at wavelength λ_k:

$$\rho(\lambda_j, \lambda_k) = \sqrt{\frac{\mathbf{n}_k^0}{\mathbf{n}_j^0}} \frac{\mathrm{cov}(\lambda_j, \lambda_k)}{\sigma(\lambda_j)\sigma(\lambda_k)} \tag{6}$$

Here the factor $(\mathbf{n}_k^0/\mathbf{n}_j^0)^{1/2}$ accounts for differing initial abundances of the two species. Figure 4d displays changes with time in the deduced fraction of (7,6) population aggregated with four other (n,m) species. Note that these

DOI: 10.1021/acs.jpclett.5b01835
J. Phys. Chem. Lett. 2015, 6, 3976−3981

fractions can add to more than one if particles contain multiple nanotubes. We find that the loose aggregates induced by salt addition are fragile enough to be disrupted by simple manual shaking, although aggregates detected as increasing covariance peaks in toluene solutions of SWCNTs wrapped with poly(9,9-di-*n*-octylfluorenyl-2,7-diyl), or PFO, appear much more robust, requiring tip sonication for disruption. Further studies should reveal whether the loose aggregates found here are precursors to tight nanotube bundles. Because nanotubes cannot be structurally sorted unless they are individualized, our covariance method for sensitively detecting aggregates may prove valuable in optimizing the conditions used in SWCNT separation processes.

Apart from its capabilities for revealing concentrations, emissive efficiencies, and aggregation in heterogeneous samples, variance spectroscopy can also isolate the spectra of homogeneous subpopulations, thereby serving to bridge the regimes of bulk and single-particle spectroscopy. In principle, the method can be extended to other optical spectroscopies, applied to solid as well as liquid phase samples, and used to analyze spectral variations in time instead of space (for liquids). Finally, variance spectroscopy should be applicable beyond carbon nanotubes to other systems, such as quantum dots, with spectral heterogeneity arising from structural polydispersity. We expect that it will prove a powerful and accessible tool for a wide range of nanoparticle studies.

EXPERIMENTAL METHODS

Approximately 5 mg of raw HiPco SWCNTs (Rice University, batch 195.1) was suspended in 10 mL of 1% sodium deoxycholate (DOC) using 30 min of bath sonication (Sharpertek Stamina XP) followed by 20 min of tip sonication (Misonix Microson XL) at a power of 7 W. The suspension was then centrifuged at 268 000*g* for 2 h and the supernatant was removed for analysis. For the aggregation study, a similar procedure was applied to prepare a SWCNT suspension in 1% sodium dodecyl sulfate (SDS). Nanotube dispersions were typically diluted by a factor of ∼5 before analysis.

Flowing Sample Apparatus. Measurements were made using a prototype model NS2 NanoSpectralyzer (Applied NanoFluorescence), an automated nanotube fluorometer. An optical schematic of the instrumental setup for variance measurements is shown in Figure S4. The sample was excited with one of three fixed wavelength diode lasers (642, 659, and 784 nm) using excitation powers that ranged from 40 to 80 mW depending on the wavelength. The resulting sample emission was collected in the backward direction and transmitted by optical fiber to the input of a SWIR spectrometer (Bruker Optics) with a thermoelectrically cooled 512-element InGaAs detector and a spectral range of approximately 900 to 1600 nm. The detector temperature was kept near −17 °C to reduce dark current noise.

Intensity fluctuations were observed from small, distinct spatial regions of the sample by passing the SWCNT suspension through a flow cuvette that had a 100 μm optical path length. Our simple gravity-driven flow apparatus is shown in Figure S4. The nanotube sample was initially placed in the upper Eppendorf tube, from which it spontaneously flowed down the connected tubing, through the flow cuvette, and then into the collection chamber. The flow rate was controlled by adjusting the vertical distance between the two Eppendorf tubes. For every sample analysis, ∼ 2000 sequential fluorescence spectra were acquired using 150 ms exposure times separated by 200 ms of dead time.

Step-Scan Apparatus. As an alternative to the flowing sample method, we constructed a separate apparatus in which the sample was loaded into a thin demountable cuvette (Precision Cells Type 20, 100 μm optical path length) that was mounted on a computer-controlled translation stage. A diode laser module (Power Technology, Inc.) emitting 82 mW at 660 nm in a circularized beam was used to excite the sample. An achromatic quarter-wave retardation plate (Thorlabs) converted the laser polarization from linear to circular to suppress any intensity variations caused by SWCNT rotation. Two short-pass filters (875 and 1100 nm, Edmund Optics) were placed in the beam path to remove any weak SWIR emission from the laser module. The beam then passed through a 2 mm hole in a reflective beam coupler and was focused into the sample by a fused silica aspheric lens (EFL = 8.0 mm, NA = 0.63, Edmund Optics). Sample emission was collected in epifluorescence geometry by the same lens and reflected by the beam coupler through an 850 nm long-pass filter (Newport) into a fiber collimator (f = 11 mm, Thorlabs). A multimode optical fiber with 300 μm core diameter and 0.39 NA transmitted the collected sample emission to the entrance slit of an SWIR spectrometer (B&WTek Sol 1.7) with a thermoelectrically cooled 512 channel InGaAs detector array and a spectral range of 840 to 1650 nm.

Step-Scan Data Acquisition. After a spectrum was acquired at a particular position, the sample cuvette was translated under computer control to a new location and halted for the next acquisition. The XYZ stages (PI model M-111.12S) were driven by a stepper motor controller (PI model Apollo C-630.23) under the control of custom LabVIEW software. In a typical experiment, spectra were measured sequentially at 86 evenly spaced points separated by 35 μm within the sample cuvette to ensure spatially independent measurements. After the last of these acquisitions, the translation stage returned to the first point and repeated the sequence of spectral measurements, revisiting the same set of positions. (Diffusion randomized the sample compositions at these positions during the time between visits.) To avoid mechanical backlash errors, scans were made in the same direction. Each of the 86 positions was visited 25 times for a total of 2150 spectra in an experimental data set. In order to minimize exposure of the sample to the excitation beam, the laser was kept off during cuvette motion and enabled only when the translation stage was halted. Mean and variance spectra were calculated separately for each of the 86 positions to suppress artifacts from cell irregularities. The sets of mean and variance spectra were then averaged together to obtain overall mean and variance spectra for the run.

ASSOCIATED CONTENT

Supporting Information

The Supporting Information is available free of charge on the ACS Publications website at DOI: 10.1021/acs.jpclett.5b01835.

Details of data analysis, derivation of covariance spectral profiles, experimental details, laser stability tests, dilution tests, and plots showing aggregation-induced changes of a covariance spectral peak (PDF)

DOI: 10.1021/acs.jpclett.5b01835
J. Phys. Chem. Lett. 2015, 6, 3976−3981

AUTHOR INFORMATION

Corresponding Author

*E-mail: weisman@rice.edu.

Present Address

§(J.K.S.) Materials Science and Engineering Division, National Institute of Standards and Technology, 100 Bureau Drive, Gaithersburg, MD 20899, USA

Notes

The authors declare the following competing financial interest(s): R.B.W. has a financial interest in Applied NanoFluorescence, LLC, which manufactures one of the instruments used in this study.

ACKNOWLEDGMENTS

This research was sponsored by the National Science Foundation (Grant CHE-1409698) and the Welch Foundation (Grant C-0807). S.R.S. is grateful to the National Science Foundation for support through an AGEP-GRS award (CHE-1401269) and the IRISE training program at Rice University (EHR-0966303).

REFERENCES

(1) Elson, E. L.; Magde, D. Fluorescence Correlation Spectroscopy.I. Conceptual Basis and Theory. *Biopolymers* **1974**, *13*, 1−27.

(2) Magde, D.; Elson, E. L.; Webb, W. W. Fluorescence Correlation Spectroscopy. II. An Experimental Realization. *Biopolymers* **1974**, *13*, 29−61.

(3) Kask, P.; Palo, K.; Ullmann, D.; Gall, K. Fluorescence-Intensity Distribution Analysis and Its Application in Biomolecular Detection Technology. *Proc. Natl. Acad. Sci. U. S. A.* **1999**, *96*, 13756−13761.

(4) Van Orden, A.; Fogarty, K.; Jung, J. Fluorescence Fluctuation Spectroscopy: A Coming of Age Story. *Appl. Spectrosc.* **2004**, *58*, 122−137.

(5) O'Connell, M. J.; Bachilo, S. M.; Huffman, C. B.; Moore, V.; Strano, M. S.; Haroz, E.; Rialon, K.; Boul, P. J.; Noon, W. H.; Kittrell, C.; et al. Band-Gap Fluorescence From Individual Single-Walled Carbon Nanotubes. *Science* **2002**, *297*, 593−596.

(6) Bachilo, S. M.; Strano, M. S.; Kittrell, C.; Hauge, R. H.; Smalley, R. E.; Weisman, R. B. Structure-Assigned Optical Spectra of Single-Walled Carbon Nanotubes. *Science* **2002**, *298*, 2361−2366.

(7) Weisman, R. B.; Bachilo, S. M. Dependence of Optical Transition Energies on Structure for Single-Walled Carbon Nanotubes in Aqueous Suspension: An Empirical Kataura Plot. *Nano Lett.* **2003**, *3*, 1235−1238.

(8) Reich, S.; Thomsen, C.; Maultzsch, J. *Carbon Nanotubes: Basic Concepts and Physical Properties*; Wiley-VCH: Weinheim, Germany, 2004.

(9) Qian, H.; Elson, E. L. Distribution of Molecular Aggregation by Analysis of Fluctuation Moments. *Proc. Natl. Acad. Sci. U. S. A.* **1990**, *87*, 5479−5483.

(10) Qian, H.; Elson, E. L. On the Analysis of High Order Moments in Fluorescence. *Biophys. J.* **1990**, *57*, 375−380.

(11) Rocha, J.-D. R.; Bachilo, S. M.; Ghosh, S.; Arepalli, S.; Weisman, R. B. Efficient Spectrofluorimetric Analysis of Single-Walled Carbon Nanotube Samples. *Anal. Chem.* **2011**, *83*, 7431−7437.

(12) Schwille, P.; Meyer-Almes, F. J.; Rigler, R. Dual-Color Fluorescence Cross-Correlation Spectroscopy for Multicomponent Diffusional Analysis in Solution. *Biophys. J.* **1997**, *72*, 1878−1886.

(13) Heinze, K. G.; Jahnz, M.; Schwille, P. Triple-Color Coincidence Analysis: One Step Further in Following Higher Order Molecular Complex Formation. *Biophys. J.* **2004**, *86*, 506−516.

(14) Burkhardt, M.; Heinze, K. G.; Schwille, P. Four-Color Fluorescence Correlation Spectroscopy Realized in a Grating-Based Detection Platform. *Opt. Lett.* **2005**, *30*, 2266−2268.

(15) Bestvater, F.; Seghiri, Z.; Kang, M. S.; Groner, N.; Lee, J. Y.; Im, K. B.; Wachsmuth, M. EMCCD-Based Spectrally Resolved Fluorescence Correlation Spectroscopy. *Opt. Express* **2010**, *18*, 23818−23828.

(16) Noda, I. Two-Dimensional Infrared (2D IR) Spectroscopy: Theory and Applications. *Appl. Spectrosc.* **1990**, *44*, 550−561.

(17) Noda, I.; Dowrey, A. E.; Marcoli, C.; Story, G. M.; Ozaki, Y. Generalized Two-Dimensional Correlation Spectroscopy. *Appl. Spectrosc.* **2000**, *54*, 236−248.

(18) Tsyboulski, D. A.; Bachilo, S. M.; Weisman, R. B. Versatile Visualization of Individual Single-Walled Carbon Nanotubes With Near-Infrared Fluorescence Microscopy. *Nano Lett.* **2005**, *5*, 975−979.

(19) Niyogi, S.; Boukhalfa, S.; Chikkannanavar, S. B.; McDonald, T. J.; Heben, M. J.; Doorn, S. K. Selective Aggregation of Single-Walled Carbon Nanotubes Via Salt Addition. *J. Am. Chem. Soc.* **2007**, *129*, 1898−1899.

(20) Lefebvre, J.; Finnie, P. Photoluminescence and Forster Resonance Energy Transfer in Elemental Bundles of Single-Walled Carbon Nanotubes. *J. Phys. Chem. C* **2009**, *113*, 7536−7540.

(21) Tan, P. H.; Rozhin, A. G.; Hasan, T.; Hu, P.; Scardaci, V.; Milne, W. I.; Ferrari, A. C. Photoluminescence Spectroscopy of Carbon Nanotube Bundles: Evidence for Exciton Energy Transfer. *Phys. Rev. Lett.* **2007**, *99*, 137402−137404.

(22) Choi, J. H.; Strano, M. S. Solvatochromism in Single-Walled Carbon Nanotubes. *Appl. Phys. Lett.* **2007**, *90*, 223114−1−223114−3.

(23) Jones, M.; Engtrakul, C.; Metzger, W. K.; Ellingson, R. J.; Nozik, A. J.; Heben, M. J.; Rumbles, G. Analysis of Photoluminescence From Solubilized Single-Walled Carbon Nanotubes. *Phys. Rev. B: Condens. Matter Mater. Phys.* **2005**, *71*, 115426-1−115426-9.

DOI: 10.1021/acs.jpclett.5b01835
J. Phys. Chem. Lett. 2015, 6, 3976−3981